PCCP

PAPER

View Article Online
View Journal | View Issue

Cite this: *Phys. Chem. Chem. Phys.*, 2015, **17**, 23392

Born–Oppenheimer and Renner–Teller coupled-channel quantum reaction dynamics of $O(^3P) + H_2^+(X^2\Sigma_g^+)$ collisions

Pablo Gamallo,*[a] Paolo Defazio,[b] Miguel González,*[a] Miguel Paniagua[c] and Carlo Petrongolo[d]

We present Born–Oppenheimer (BO) and Renner–Teller (RT) time dependent quantum dynamics studies of the reactions $O(^3P) + H_2^+(X^2\Sigma_g^+) \rightarrow OH^+(X^3\Sigma^-) + H(^2S)$ and $OH(X^2\Pi) + H^+$. We consider the OH_2^+ $\tilde{X}^2A''$ and $\tilde{A}^2A'$ electronic states that correlate with a linear $^2\Pi$ species. The electronic angular momenta operators $\hat{L}$ and $\hat{L}^2$ are considered in nonadiabatic coupled-channel calculations, where the associated RT effects are due to diagonal V^{RT} potentials that add up to the PESs and to off-diagonal C^{RT} couplings between the potential energy surfaces (PESs). Initial-state-resolved reaction probabilities P_I, integral cross sections σ_I, and rate constants k_I are obtained using recent *ab initio* PESs and couplings and the real wavepacket formalism. Because the PESs are strongly attractive, P_I have no threshold energy and are large, σ_I decrease with collision energy, and k_I depend little on the temperature. The $\tilde{X}^2A''$ PES is up to three times more reactive than the $\tilde{A}^2A'$ PES and H_2^+ rotational effects (j_0 = 0, 1) are negligible. The diagonal V^{RT} potentials are strongly repulsive at the collinearity and nearly halve all low-energy observables with respect to the BO ones. The off-diagonal C^{RT} couplings are important at low partial waves, where they mix the $\tilde{X}^2A''$ and $\tilde{A}^2A'$ states up to ~20%. However, V^{RT} effects predominate over the C^{RT} ones that change at most by ~19% the BO values of σ_I and k_I. The reaction $O(^3P) + H_2^+(X^2\Sigma_g^+) \rightarrow OH^+(X^3\Sigma^-) + H(^2S)$ is probably one of the most reactive atom + diatom collisions because its RT rate constant at room temperature is equal to 2.26×10^{-10} cm^3 s^{-1}. Within the BO approximation, the present results agree rather well with recent quasiclassical and centrifugal-sudden data using the same PESs.

Received 15th June 2015,
Accepted 10th August 2015

DOI: 10.1039/c5cp03451e

www.rsc.org/pccp

I. Introduction

The atom–molecular ion reactions

$$O(^3P) + H_2^+(X^2\Sigma_g^+) \rightarrow OH^+(X^3\Sigma^-) + H(^2S), \quad \Delta D_0 = -2.44 \text{ eV}$$
proton transfer, H channel, (1.1)

$$\rightarrow OH(X^2\Pi) + H^+, \quad \Delta D_0 = -1.74 \text{ eV}$$
hydrogen transfer, H^+ channel, (1.2)

can play a significant role in atmospheric elementary processes, where the OH_2^+ reaction intermediate is produced by water ionization and was observed since 1974.[1–3] Although the water molecule and related ionic species (O^+, OH^+, H_2O^+, H_3O^+, *etc.*) are important in the astrochemical context, it should be noted that the importance of reactions (1.1) and (1.2) in astrochemistry is still unclear.[4] Moreover, the $O(^3P) + H_2^+(X^2\Sigma_g^+)$ system is related to other interesting ionic systems as, *e.g.*, the $X(^1S) + H_2^+ \rightarrow XH^+ + H$ (X = He, Ne, Ar) and $O^+(^4S) + H_2 \rightarrow OH^+ + H$ reactions.[5,6]

The dynamics of the collisions (1.1) and (1.2) was investigated in an old experimental work reported by McClure *et al.*[7] for the deuterated variant D_2^+, and in some very recent theoretical contributions by Paniagua *et al.*,[8] Martínez *et al.*,[9] and Gannouni *et al.*[10] We plot schematically in Fig. 1 the relevant electronic correlation diagram, simplifying those of ref. 8 and 11 and using the energies given in ref. 8. The two lowest potential energy surfaces (PESs) are barrierless and present strongly bound minima at −8.16 and −7.54 eV with respect to the reactants. The product channels (1.1) and (1.2) are uncoupled within the adiabatic Born–Oppenheimer (BO) approximation and occur, respectively, on the two lowest $\tilde{X}^2A''$ and $\tilde{A}^2A'$ PESs of OH_2^+, which transform as $^2B_1$ and $^2A_1$, respectively, in C_{2v} symmetry.

The ground PES ($\tilde{X}^2A''$) includes the ground electronic state of the water cation, $H_2O^+(\tilde{X}^2B_1)$, in the minimum energy path

[a] *Departament de Química Física i Institut de Química Teòrica i Computacional, Universitat de Barcelona, C/ Martí i Franquès 1, 08028 Barcelona, Spain. E-mail: gamallo@ub.edu, miguel.gonzalez@ub.edu*
[b] *Dipartimento di Biotecnologie, Chimica, e Farmacia, Università di Siena, Via A. Moro 2, 53100 Siena, Italy*
[c] *Departamento de Química Física Aplicada, Universidad Autónoma de Madrid, C/ Francisco Tomás y Valiente 7, 28049 Cantoblanco, Spain*
[d] *Istituto per i Processi Chimico Fisici, Consiglio Nazionale delle Ricerche, Via G. Moruzzi 1, 56124 Pisa, Italy*

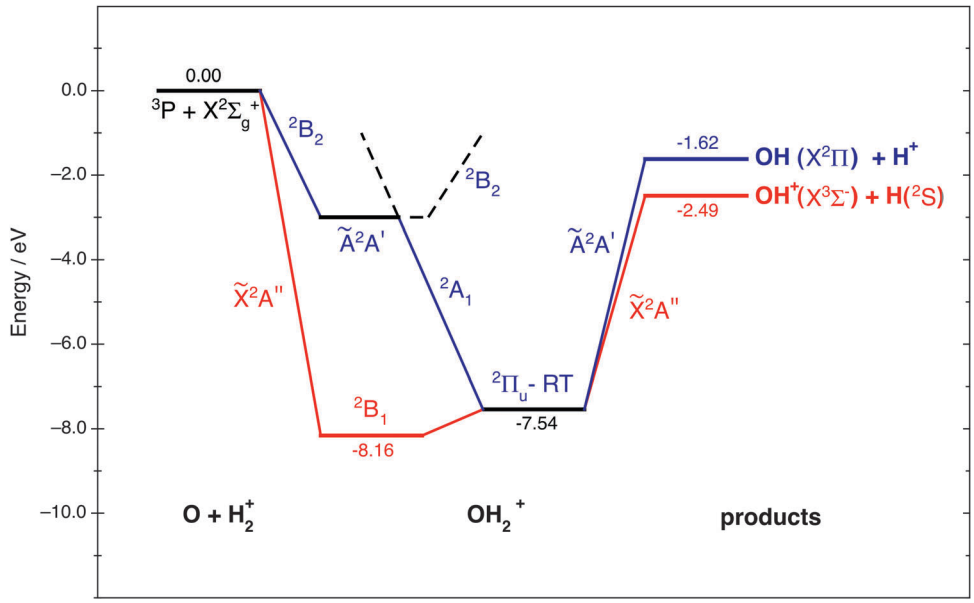

Fig. 1 Correlation diagram of OH_2^+ $\tilde{X}^2A''$ ($^2B_1$, red) and $\tilde{A}^2A'$ ($^2A_1$, blue).

(MEP) connecting reactants and OH^+ + H products; while the first excited PES ($\tilde{A}^2A'$) includes the first excited electronic state of the water cation, $H_2O^+(\tilde{A}^2A_1)$, in the MEP involving reactants and OH + H^+ products. These two electronic states of H_2O^+ correspond to the degenerate components of a $^2\Pi_u$ species, when the molecule is in a linear arrangement, and the associated nonadiabatic (NA) Renner–Teller (RT) effects can remarkably influence the dynamics of these collisions, as they also occur for the $\tilde{X}^2B_1 - \tilde{A}^2A_1$ optical spectrum[12] of H_2^+O.

This is especially important here because the deep potential wells and $^2\Pi$ configurations are geometrically and energetically close and most collisions proceed *via* OH_2^+ intermediate collision-complexes.[8,9] When the RT interactions are large, we really have two coupled reactions (1.1) and (1.2) that mainly proceed on both interacting PESs. The contribution of the $^2A_1 - {}^2B_2$ conical-intersection to the dynamics has not been considered in this work, and its influence has been recently studied in the photodissociation of H_2O^+ of ref. 13.

The $\tilde{X}^2A''$ and $\tilde{A}^2A'$ PESs are based on *ab initio* calculations[8] at the internally-contracted multi-reference configuration-interaction level, employing the Davidson correction (icMRCI + Q) and the augmented correlation-consistent polarized-valence quadruple-zeta basis set (aug-cc-pvQZ). More than 2000 *ab initio* points of both PESs were then fitted to a many-body expansion. Paniagua *et al.*[8] also obtained BO quasiclassical trajectories (QCTs), integral cross sections, and thermal rate constants of both reactions and of their deuterated variants (D_2^+ and HD^+) on both PESs. Following that work, Martínez *et al.*[9] employed the quantum-mechanical real wavepacket (RWP) method to obtain BO centrifugal-sudden (CS) initial-state-selected reaction probabilities and cross sections. Large reaction probabilities and decreasing cross sections were obtained for both reaction channels. Channel (1.1) was found to be nearly three times more reactive than (1.2).

Extending the previous studies,[8,9] the present paper reports a RWP study of the dynamics of the (1.1) and (1.2) collisions, at the NA RT coupled-channel (CC) level. We employ the OH_2^+ $\tilde{X}^2A''$ and $\tilde{A}^2A'$ PESs of ref. 8 and the NH_2 RT matrix elements of Zhou *et al.*,[14] taking into account that these triatoms are isoelectronic and have similar rovibronic structures.[12] The RT matrix elements were already employed by Zhou *et al.*[14] and by Lin *et al.*[15] in NH_2 and $N(^2D) + H_2(X^1\Sigma_g^+)$ spectroscopic and collisional studies, respectively. Obviously, the results obtained in this study can be useful for a first estimation of quantum dynamical properties taking into account the presence of nonadiabatic effects in the title reactions. Nevertheless, higher accuracy could be reached once the RT matrix elements for this reaction are explicitly calculated, although small differences between both systems are expected.

The paper is organized as follows. Section II presents some theoretical and computational details, enlightening the origin, formulae, and physical meanings of the adiabatic (diagonal) and nonadiabatic (off diagonal) RT terms. Section III reports initial-state-resolved reaction probabilities for the lowest rotational states of H_2^+ in the ground vibrational state, and for the product reaction channels (1.1) and (1.2). We take into account many total angular momentum quantum numbers J, both overall parities $p = \pm$, and the Coriolis couplings among all $K \geq 0$ projections of J along the O–(H_2^+) axis. We report initial-state-resolved integral cross sections and rate constants in Section IV, discussing the influence of the RT effects on both product channels and comparing our BO results with previous QCT[8,9] and RWP CS[9] calculations and we, finally, present in Section V the main conclusions.

II. Theory and calculation details

Following our previous studies,[16–18] the triatomic system ABC is described by the reactant A + BC Jacobi coordinates (R, r, and γ),

a body-fixed reference frame with the z axis along R, a spinless rovibronic Hamiltonian $\hat{H}$ that contains both the total $\hat{J}$ and the electronic $\hat{L}$ angular momentum, and the $C_s(M)$ or $C_{2v}(M)$ permutation-inversion groups that are isomorphic with the C_s or C_{2v} point groups, respectively. As usual, we employ atomic units unless stated otherwise.

The largest RT effects are due to the matrix elements of $\hat{L}_R^2$ or $\hat{L}_R$, which are respectively diagonal or off-diagonal in an adiabatic electronic representation $|\sigma\Lambda\rangle$ with parity $\sigma = \pm$ and orbital angular momentum quantum number $\Lambda \geq 0$ at the linearity. Omitting the $\hat{L}_\pm$ minor contributions, $\hat{H}$ contains the $\hat{L}_R^2/\sin^2\gamma$, $\hat{J}_R\hat{L}_R/\sin^2\gamma$, and $\hat{J}_\pm\hat{L}_R\cot\gamma$ operators, and the RT effects are thus responsible for the coupling among three degrees of freedom: the electronic and total rotations around R and the angular motion. The OH_2^+ electronic states are $|-1\rangle$ = $\tilde{X}^2A''$ and $|+1\rangle$ = $\tilde{A}^2A'$ (or $\tilde{X}^2B_1$ and $\tilde{A}^2A_1$ in C_{2v}, respectively). Eqn (3) of ref. 18 shows that the electronic matrix elements of $\hat{L}_R^2$ and $\hat{L}_R$ define two different contributions to the RT effect.

The former RT term is associated with $\hat{L}_R^2$ and is defined by the diagonal potentials

$$V_\sigma^{RT} = \frac{B\cos^2\gamma + b}{\sin^2\gamma}\langle\sigma\Lambda|\hat{L}_R^2|\sigma\Lambda\rangle, \qquad (2.1)$$

where B and b are half the inverse inertial moments associated with R and r, respectively. These potentials add up to the usual BO PESs, thus generalizing the BO approximation, and present RT barriers that diverge at the linearity. Therefore, these RT terms inhibit the reactivity with respect to the BO one, provided the collision samples quasilinear geometries. This preferably occurs when the $K = 0$ component of the wavepacket predominates, because the Legendre polynomials $|j0\rangle$ are maximal at the linearity.

The latter RT term is due to $\hat{L}_R$ and to the real, symmetrical, and (J,K)-dependent off-diagonal couplings

$$C_{-\sigma\sigma}^{RT} = \sigma i\langle-\sigma\Lambda|\hat{L}_R|\sigma\Lambda\rangle\left\{\delta_{K'K}2K\frac{B\cos^2\gamma + b}{\sin^2\gamma} + B\cot\gamma\left[\delta_{K',K+1}(1+\delta_{K0})^{1/2}\lambda_{JK}^{+} + \delta_{K',K-1}(1+\delta_{K1})^{1/2}\lambda_{JK}^{-}\right]\right\}, \qquad (2.2)$$

where $\lambda_{JK}^{\pm} = [J(J+1) - K(K\pm1)]^{1/2}$. This equation contains three terms: the first is K-diagonal and the other two involve the RT–Coriolis interaction. When K or $K' > 0$, these terms are different from zero and account for both the breakdown of the BO approximation and the nonadiabatic interactions between the electronic states. These couplings also diverge at the linearity if $K' = K$.

Considering H_2^+ in the ground vibrational state, $\nu_0 = 0$, we calculate BO and RT coupled-channel (CC) initial-state-resolved reaction probabilities $P^{Jp}_{e_0j_0K_0}(E_{col})$, where e_0 and (j_0,K_0) label the initial OH_2^+ electronic and H_2^+ rotational state, respectively, and E_{col} is the collision energy. We here consider $j_0 = 0$ and 1, E_{col} from 0.05 to 0.4 eV, $J \leq 75$, and the Coriolis couplings among all K projections. Some checks performed until $J = 30$ showed that the deep minima involved in this study make necessary the propagation of the full set of K projections. At higher J values a similar behavior is expected according to the general trend observed in insertion reactions occurring through a deep minimum along the MEP.[19,20]

The reaction probabilities are obtained through the real wavepacket (RWP) formalism of Gray and Balint-Kurti,[21,22] *via* a scaled and shifted Hamiltonian $\hat{H}_s$, solving an arccos mapping of the equation of motion. We employ an initial complex Gaussian WP, $|\psi_0\rangle = |a_0\rangle + i|b_0\rangle$, with the R-dependent part given by

$$g_0(R) = \pi^{-1/4}\alpha^{-1/2}e^{-(R-R_0)^2/2\alpha^2}e^{-\frac{i}{\hbar}(2\mu_R E_0)^{1/2}(R-R_0)}, \qquad (2.3)$$

where μ_R is the reduced mass associated with R and E_0 is the initial collision energy. The main equations to solve are[21]

$$|a_1\rangle = \hat{H}_s|a_0\rangle - (1-\hat{H}_s^2)^{1/2}|b_0\rangle, \quad \text{first propagation (complex WP)}, \qquad (2.4)$$

$$|a_{n+2}\rangle = 2\hat{H}_s|a_{n+1}\rangle - |a_n\rangle, \quad \text{other propagations (real WP)}. \qquad (2.5)$$

The calculations are performed using reactant Jacobi coordinates, the square root involving the $\hat{H}_s$ operator is evaluated *via* a Chebyshev expansion, and eqn (2.5) corresponds to a standard Chebyshev propagation of just a real WP, which is damped at large R and r values by the Gaussians of eqn (28) and (29) of ref. 21. At the end of the propagations, the reaction probabilities are obtained through a flux method.[22] The RWP method shares common features with the time independent studies of Chen and Guo[23] and Kroes and Neuhauser,[24] and it is essentially coincident with the Chebyshev WP approach of Lin and Guo.[25]

We propagate CC WPs at $J \leq 10$, $J = 30$, 50, 60, 65, 70, and 75, according to the numerical parameters of Table 1, which correspond to 6 042 330 basis states for each electronic species at $J = 0$, converging the probabilities in the range E_{col} = 0.05–0.4 eV within 2% and 40 000 iterations. Owing to the high cost of RT CC calculations and the usual J shifts of the probability thresholds, we employ a J fitting-interpolation technique[19] at any (j_0,K_0) pair for obtaining reaction probabilities $P^{Jp}_{e_0j_0K_0}(E_{col})$ at all non-propagated WP J values. The comparison with some CC data shows that this approach gives good results for probabilities and cross sections, and error bars of $\sim$2% for room-temperature rates, as Fig. 7 of ref. 20 shows for the conical-intersection collision $OH(A^2\Sigma^+) + H(^2S)$.

Table 1 Parameters of the quantum dynamics calculations. Values in atomic units, unless otherwise specified

Initial Gaussian $g_0(R)$	
Width α, R_0 center, and E_0 translational energy	0.3, 30, and 0.4 eV
R range and number of grid points	0–37 and 417
r range and number of grid points	0.5–18.5 and 207
Associated Legendre functions $\|jK\rangle$, j_{max}	140[a]
R and r absorption start at	32 and 13.5
Absorption strength	0.0005
Flux analysis at r	12.5

[a] Due to the symmetry of the system this corresponds to 70 j values and γ points.

Cross sections $\sigma_{e_0 j_0}(E_{\rm col})$ and rate constants $k_{e_0 j_0}(T)$, in the temperature range T = 200–900 K, are obtained through the usual expressions

$$\sigma_{e_0 j_0}(E_{\rm col}) = \frac{\pi}{(2j_0+1)2\mu_R E_{\rm col}} \sum_J (2J+1) \sum_p \sum_{K_0}^{\min(j_0,J)} P^{Jp}_{e_0 j_0 K_0}(E_{\rm col}), \quad (2.6)$$

$$k_{e_0 j_0}(T) = f_{\rm el} \left(\frac{8}{\pi \mu_R k_{\rm B}{}^3 T^3}\right)^{1/2} \int_0^\infty E_{\rm col} \exp(-E_{\rm col}/k_{\rm B}T) \sigma_{e_0 j_0}(E_{\rm col}) {\rm d}E_{\rm col}, \quad (2.7)$$

where $f_{\rm el}$ is the population of the initial electronic state e_0 and depends on the electronic partition functions,

$$f_{\rm el} = q_{{\rm el},e_0} \Big/ q_{{\rm el},{\rm O}(^3{\rm P})} q_{{\rm el},{\rm H_2}^+(\tilde{\rm X}^2\Sigma_g^+)} = 1 \Big/ q_{{\rm el},{\rm O}(^3{\rm P})}. \quad (2.8)$$

Because the doublet PESs were calculated without accounting for the O(^3P_M) spin–orbit (SO) interaction, three different and approximate strategies can be employed for estimating the O(^{3}P) partition function:

(1) $q^{(1)}_{{\rm el},{\rm O}(^3{\rm P})} = 9$ without fine structure, in a fully consistent way with the PES calculation.

(2) $q^{(2)}_{{\rm el},{\rm O}(^3{\rm P})} = \sum_M (2M+1)\exp(-\varepsilon_M/k_{\rm B}T)$, with the SO energy levels[26] ε_2 = 0, ε_1 = 158, and ε_0 = 227 cm^{-1} referred to the ground state O($^3P_2$), and with $q_{{\rm el},{\rm O}(^3{\rm P})}$ increasing with T from 5 to 9. This is the usual procedure which is not, however, strictly consistent with the PES calculation.

(3) $q^{(3)}_{{\rm el},{\rm O}(^3{\rm P})} = \sum_M (2M+1)\exp(-\varepsilon_M{}'/k_{\rm B}T)$, with $\varepsilon_2{}'$ = −78, $\varepsilon_1{}'$ = 80, and ε_0 = 149 cm^{-1} referred to the O(^{3}P) term.[8] This proposal[27,28] agrees with the energy zero at the O(^{3}P) + H_2^+ asymptote without SO and can give a better agreement with the experiment.[29] However, $q^{(3)}_{{\rm el},{\rm O}(^3{\rm P})}$ is not fully meaningful, because it evolves from a divergent value at low T up to 9 at high T, and it is not consistent with the PESs.

In conclusion, the first choice is both fully consistent and physical and we therefore propose using $f_{\rm el}$ = 1/9 through this study, although the other choices are also depicted once for comparison. The H and H^+ channels correspond to the cross sections $\sigma^{\rm H}_{{\rm X}j_0}$ and $\sigma^{{\rm H}^+}_{{\rm A}j_0}$ in the BO approximation, respectively, but they are associated with $\sigma^{\rm H}_{j_0} = \sigma^{\rm H}_{{\rm X}j_0} + \sigma^{\rm H}_{{\rm A}j_0}$ and $\sigma^{{\rm H}^+}_{j_0} = \sigma^{{\rm H}^+}_{{\rm X}j_0} + \sigma^{{\rm H}^+}_{{\rm A}j_0}$ at the RT level, where the $\sigma^{\rm H}_{{\rm A}j_0}$ and $\sigma^{{\rm H}^+}_{{\rm X}j_0}$ cross sections are due to the nonadiabatic couplings $C^{\rm RT}$ of eqn (2.2). Analogous expressions can be considered for the rate constants.

Note that the parameters of Table 1 produce reliable results just for $E_{\rm col} \geq 0.05$ eV and that their use at lower energies can give wrong cross sections for the O + H_2^+ ionic collision. In principle, this drawback can be removed using other initial WPs below 0.05 eV, with larger α, R_0, and radial grids, as we did for the H + HeH^+ reaction,[30] where these modifications described were able to reproduce with high accuracy the close coupling time independent results[31] also in the cold energy range. Nevertheless, considering the additional and intensive RT CC calculations that would be necessary, we follow here a simpler strategy. Guided by some time-independent quantum-dynamics calculations through the ABC code[32] and by QCT[8] results at $E_{\rm col} < 0.05$ eV, in a similar procedure to that employed for the Ne + H_2^+ reaction,[33] we fit here the WP cross sections at $E_{\rm col} \geq 0.05$ eV using the well known expression[34]

$$\sigma(E_{\rm col}) = C_{\rm s} E^{\rm s}_{\rm col}, \quad (2.9)$$

which is then employed for extrapolating σ down to $E_{\rm col}$ = 0.005 eV. Therefore, in Sections III and IV we present RWP reaction probabilities and cross sections in the range $E_{\rm col}$ = 0.05–0.4 eV, and rate constants are obtained from the above cross sections and from the extrapolated ones in the range 0.005–0.05 eV.

III. Reaction probabilities

For the reader's convenience, we remember that the product channels H, proton transfer, and H^+, hydrogen-atom transfer, eqn (1.1) and (1.2), are separated in the BO approximation, where a given collision always evolves on a single PES (the $\tilde{\rm X}^2{\rm A}''$ or the $\tilde{\rm A}^2{\rm A}'$ PES). Moreover, the single-state dynamics is affected by the $V^{\rm RT}$ potential (2.1) and the $C^{\rm RT}$ couplings (2.2) vanish identically at J = 0, when the WP remains on the initial surface.

Fig. 2 reports BO and RT reaction probabilities $P^{J-}_{\rm X00}$ and $P^{J+}_{\rm A00}$ for both channels H and H^+ and initial electronic states, at J = 0, 10, and 50, $p = -(^2{\rm A}'')$ or $+(^2{\rm A}')$, j_0 = 0, and K_0 = 0. At low J values, the BO probabilities (left panels) do not present any threshold and increase sharply up to high values, with mild oscillations around a value of ∼0.90. The resonance structure found suggests the existence of an indirect insertion mechanism, favored by the deep minima of both PESs. The formation of short-lived collision complexes that break down rather quickly towards the product channels has also been reported in QCT calculations on the same PESs.[9] As usual, high J values strongly damp the intensity of the oscillations observed, owing to the averaging effects of the Coriolis couplings among many K values, suggesting an increasing contribution of direct collisions in the process for $J \geq 30$, in agreement with QCT results.[9]

The energy thresholds depend on the $BJ(J+1)$ centrifugal barriers in the entrance valley and on the J-dependent energy shifts found on the $\tilde{\rm A}^2{\rm A}'$ excited surface, which correlates with the excited OH + H^+ products, are much larger than those found on the ground $\tilde{\rm X}^2{\rm A}''$ PES. At J = 50, for example, the $\tilde{\rm X}^2{\rm A}''$ and $\tilde{\rm A}^2{\rm A}'$ BO thresholds are equal to ∼0.05 and ∼0.20 eV, respectively. This is consistent with the $\tilde{\rm A}^2{\rm A}'$ $D_{\infty h}$ equilibrium geometry, where $B \sim R^{-2}$ can achieve large values, with a nearly collinear OHH dynamics on this excited PES, and with the larger values of the $\tilde{\rm X}^2{\rm A}''$ maximum impact parameter, $b_{\rm max}$, found in the QCT calculations.[8,9] These findings imply that O + H_2^+ collisions are very reactive and that the H product channel (proton transfer reaction) is favored with respect to the H^+ one. We anticipate that cross sections and rate constants confirm these reactivity trends and that including the RT coupling also leads to the same tendency.

The right panels of Fig. 2 show RT reaction probabilities. The J = 0 RT couplings $C^{\rm RT}$ (2.2) are identically equal to zero, as

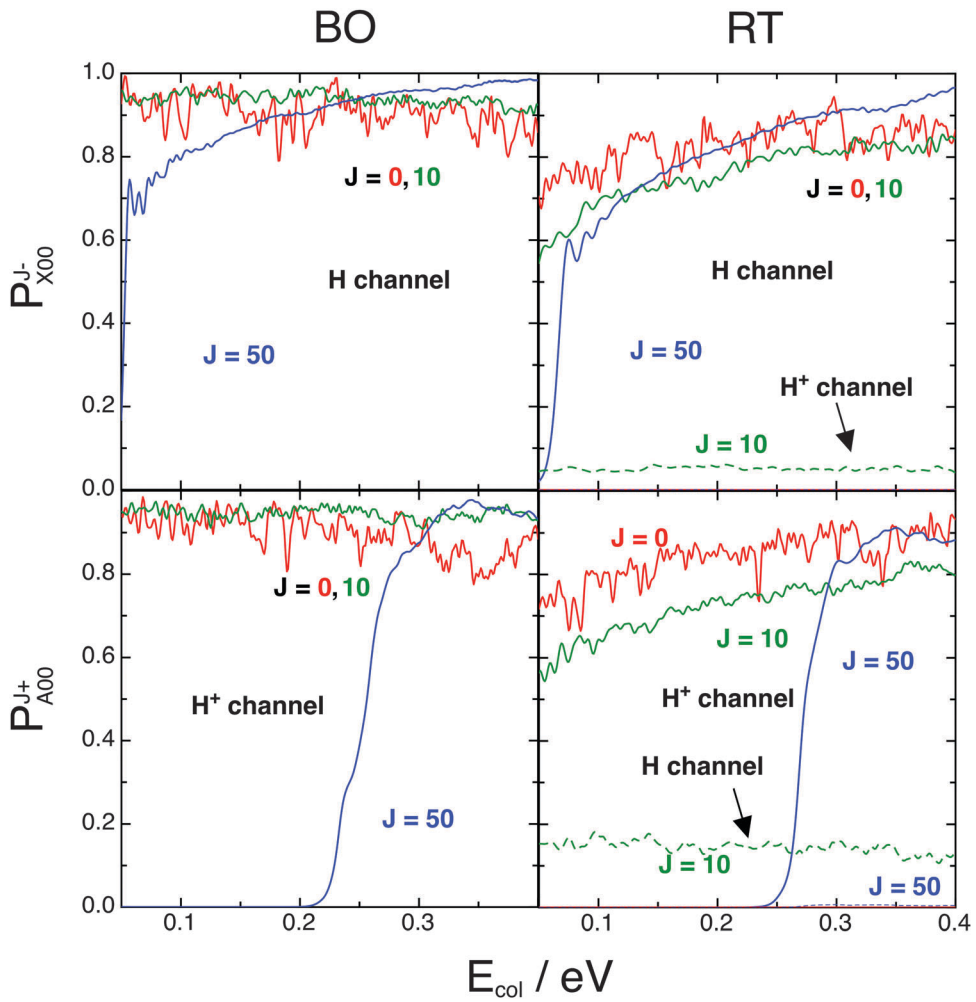

Fig. 2 BO (left) and RT (right) CC reaction probabilities. $e_0 = \tilde{X}^2A''$ (above) and $\tilde{A}^2A'$ (below). $J = 0$ (red), 10 (green), 50 (blue). $p = -$ (above) and + (below). $j_0 = 0$, $K_0 = 0$, $E_{col} \geq 0.05$ eV. Probabilities due to C^{RT} are shown as dashed lines.

previously indicated, and they are negligibly small at $J \geq 50$. The comparison of the BO and RT reaction probabilities shows that the RT coupling term increases the energy thresholds, reduces significantly the probabilities, and opens both the H and H^+ channels at $J \sim 10$. The probability lowering occurs even at $J = 0$, when the two electronic states involved are uncoupled, and it is, therefore, due to the presence of the RT potentials V_σ^{RT} (2.1). These are, in fact, quite large in a wide region of the coordinate space, owing to the $1/\sin^2\gamma$ factor when OH_2^+ is nearly linear, or due to the large $\hat{L}_R^2$ matrix elements when OH_2^+ bends.[14] At low J values, the RT couplings C^{RT} (2.2) between the two electronic states are present but are rather small. Therefore, $O + H_2^+$ collisions give preferentially $OH^+ + H$ or $OH + H^+$ products when the WP starts on the ground $\tilde{X}^2A''$ or excited $\tilde{A}^2A'$ surface, respectively. In the latter case, however, the RT effects are larger owing to the linear ($^2\Pi_u$) equilibrium geometry of the minimum. For $J > 10$, the RT diagonal terms V_σ^{RT} are still large but the off diagonal ones C^{RT} decrease and vanish at $J \sim 30$.

Consequently, the two electronic states involved are, in practice, not RT-coupled at these high partial waves, as the probabilities at $J = 50$ show. Looking at eqn (2.2), we see that this finding is probably associated with the small $\langle\tilde{X}|\hat{L}_R|\tilde{A}\rangle$ value at many geometries.[14] Dynamic effects can be also operative, with the WP evolution being strongly influenced by the K_0 initial value, in agreement with the fast collisions occurring at high-J values. For example, $K_0 = 0$ might be nearly conserved during the high-J dynamics owing to the high number of available K final states opened by RT Coriolis couplings, with $C^{RT} \sim 0$. This fact is consistent with a CS approximation that works quite well at the RT level.

We confirm this hypothesis by comparing some CC and CS reaction probabilities in Fig. 3, plotting the BO and RT $\tilde{X}^2A''$ probabilities P^{30-}_{X00} at $J = 30$, $p = -$, $j_0 = 0$, and $K_0 = 0$. Within the CS approximation, the electronic states are not RT-coupled because only the $K = K_0 = 0$ channel is open and all C^{RT} couplings (eqn (2.2)) are, therefore, identically equal to zero. Other initial conditions give essentially the same scenario. Within the BO approximation, the agreement between CC and CS results is, in general, acceptable, although the CS reaction probability is, as usual, more oscillating and somewhat smaller than the CC one. This is consistent with the CC averaging effects

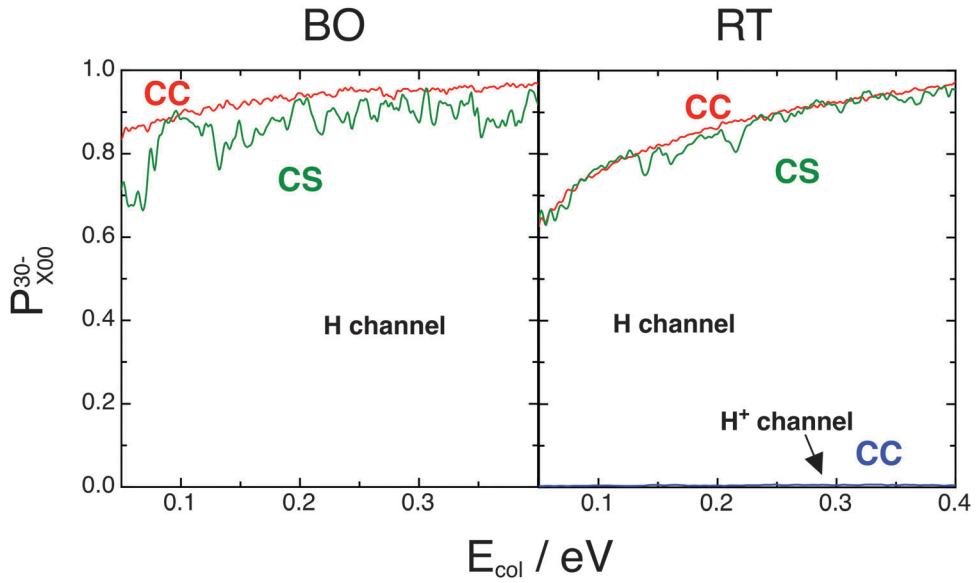

Fig. 3 BO (left) and RT (right) CC (red) and CS (green) reaction probabilities. $J = 30$, $p = -$, $e_0 = \tilde{X}^2A''$, $j_0 = 0$, $K_0 = 0$, $E_{col} \geq 0.05$ eV.

resulting from taking into account 31 K values and the moderate and negative Coriolis couplings that enhance the CC reactivity. On the other hand, the CS approximation works quite well at the RT level because the K-diagonal matrix elements of $\hat{L}_R^2/\sin^2\gamma$, eqn (2.1), predominate over the Coriolis couplings. This fact inhibits more the RT CC probability than the RT CS one that are thus nearly equal, and the initial K_0 remains approximately a good quantum number. Note also that RT CC interactions with the excited $\tilde{A}^2A'$ electronic state, leading to the $OH + H^+$ products, are fully negligible at $J = 30$.

Fig. 4 shows how the initial K_0 value affects the $O(^3P) + H_2^+$ reaction probabilities, presenting BO and RT probabilities P^{5-}_{A10} and P^{5-}_{A11} at $e_0 = \tilde{A}^2A'$, $J = 5$, $p = -$, $j_0 = 1$, and $K_0 = 0$ and 1. The BO results are nearly equal but the RT ones present significant differences depending on the K_0 values, because they correspond to the initial Legendre functions $|10\rangle \sim \cos\gamma$ or $|11\rangle \sim \sin\gamma$ for $K_0 = 0$ or 1, respectively. When $K_0 = 0$, the initial WP density is largest at $\gamma = 0$ and the RT linear barrier $\sim\langle\tilde{A}|\hat{L}_R^2|\tilde{A}\rangle/\sin^2\gamma$ strongly reduces the reactivity. In contrast, the maximum initial density of the latter WP, $K_0 = 1$, occurs at $\gamma = 90^\circ$; that is to say, along a more attractive region, where the linear barrier has a minimal contribution. Contrasting the H and H^+ reaction channels, we see that ~15–20% of the WP jumps from the initial excited surface, $\tilde{A}^2A'$, to the ground one, $\tilde{X}^2A''$, at both K_0 values.

All these results are typical of barrierless and exothermic RT collisions on bound PESs, because we found similar V^{RT} and K_0 effects in the $C(^1D) + H_2(^1\Sigma_g^+)$ collisions.[18]

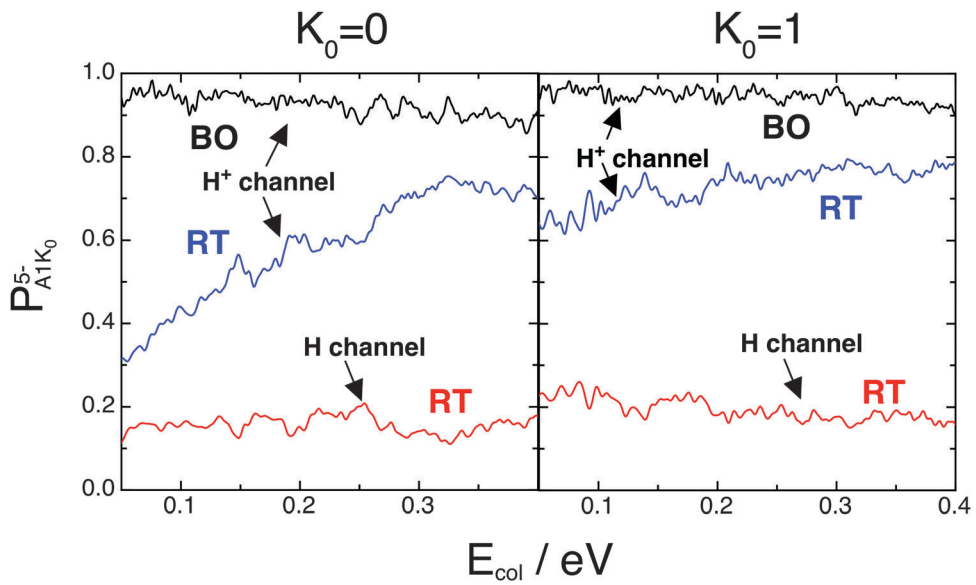

Fig. 4 BO (black) and RT (red and blue) CC reaction probabilities. $J = 5$, $p = -$, $e_0 = \tilde{A}^2A'$, $j_0 = 1$, $K_0 = 0$ (left) and 1 (right), $E_{col} \geq 0.05$ eV.

IV. Cross sections and rate constants

Fig. 5 shows the BO and RT reaction cross sections σ_{Xj_0} and σ_{Aj_0} for both channels H and H^+ and initial electronic states, at $j_0 = 0$ and 1, and Table 2 reports some representative numerical results for $j_0 = 0$. We shall first discuss BO cross sections and then show how RT effects modify the reactivity. The collision energy and rotational effects reflect the barrierless and rather isotropic character of both PESs; that is to say, the cross sections decrease with E_{col} without appreciable oscillations and are negligibly affected by the H_2^+ rotation level j_0. The ground-state BO $\sigma^{H}_{X_{j_0}}$ decreases with the collision energy faster than the excited-state BO $\sigma^{H^+}_{A_{j_0}}$. For example, Table 2 shows that the BO σ^{H}_{X0} or $\sigma^{H^+}_{A0}$ is lowered by a factor of 3.2 or 1.7, respectively, from 0.05 to 0.4 eV, suggesting that for the ground PES it is easier for the system to depart from the MEP as E_{col} increases in comparison to the excited PES.

The ground state is also more reactive than the excited one, up to ~3 times at 0.05 eV, owing to its more attractive character and larger exothermicity shown in Fig. 1, and to the smaller J shifts of the reaction probabilities in Fig. 2. Therefore, more partial waves contribute to the ground-state cross sections in the energy range investigated. As E_{col} increases, the reactivity of the electronic states becomes progressively more similar: at $j_0 = 0$, *e.g.*, the H/H^+ BO product branching ratio $\sigma^{H}_{X0}/\sigma^{H^+}_{A0}$ decreases from 2.9 to 1.5 in the E_{col} range 0.05–0.4 eV. On the overall, the proton transfer reaction giving the OH^+ + H products is preferred with respect to the hydrogen transfer one leading to OH + H^+.

The inclusion of the RT effects confirms the behavior of the cross sections with respect to the collision energy, to the initial

Table 2 H and H^+ BO and RT $j_0 = 0$ cross sections/Å^2

	H channel			H^+ channel		
E_{col}/eV	σ^{H}_{X0} BO	σ^{H}_{X0} RT	σ^{H}_{0} RT	$\sigma^{H^+}_{A0}$ BO	$\sigma^{H^+}_{A0}$ RT	$\sigma^{H^+}_{0}$ RT
0.05	153.4	98.6	103.3	53.6	30.9	32.4
0.1	105.1	80.3	83.8	44.2	29.9	31.0
0.2	69.1	57.9	59.7	36.5	29.1	29.7
0.3	54.9	50.0	51.2	33.8	28.5	28.9
0.4	48.4	44.6	46.1	32.2	27.7	28.0

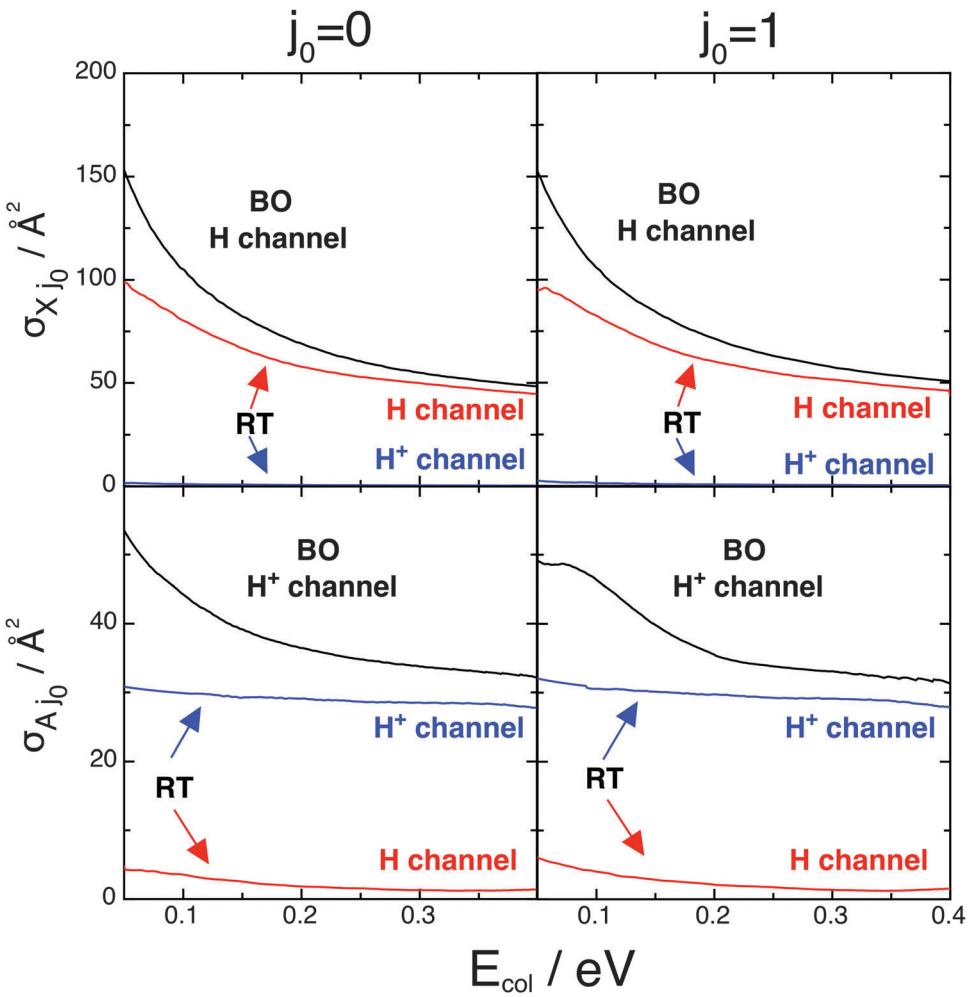

Fig. 5 BO (black) and RT (red and blue) CC cross sections. $e_0 = \tilde{X}^2A''$ (above) and $\tilde{A}^2A'$ (below), $j_0 = 0$ (left) and 1 (right), $E_{col} \geq 0.05$ eV.

electronic and rotational states, and to the product channels. The results presented in Fig. 5 and Table 2 clearly point out the differences between BO and RT treatments and the different role of the contributions to RT effects, namely the adiabatic linear barriers V^{RT} (2.1) and the nonadiabatic couplings C^{RT} (2.2) where the former is by far that predominant. In this table, $\sigma_0^H = \sigma_{X0}^H + \sigma_{A0}^H$, $\sigma_0^{H^+} = \sigma_{X0}^{H^+} + \sigma_{A0}^{H^+}$, the difference $\sigma_{e_0 0}(RT) - \sigma_{e_0 0}(BO)$ is mainly associated with V^{RT}, whereas $\sigma_{A0}^H(RT)$ and $\sigma_{X0}^{H^+}(RT)$ are essentially due to C^{RT}. In fact, the latter cross sections correspond to NA jumps from the reactant channel on the excited $\tilde{A}^2A'$ PES to the product channel on the ground $\tilde{X}^2A''$ surface (see Fig. 1), and these transitions are induced by the $\langle \tilde{X}|\hat{L}_R|\tilde{A}\rangle$ matrix element. RT cross sections are smoother than the BO ones, for example, the RT ratio $\sigma_0^H(0.05)/\sigma_0^H(0.4)$ is equal to 2.2 whereas the BO one $\sigma_{X0}^H(0.05)/\sigma_{X0}^H(0.4)$ is 3.2. In particular, RT effects decrease the reactivity of the system at low-intermediate E_{col} values, *e.g.*, it is reduced up to a factor of 1.6 with respect to the BO one at 0.05 eV. This is consistent with the probability results and is due to the diagonal RT barriers V^{RT}. The nonadiabatic couplings C^{RT} are more important when the WP starts on the excited $\tilde{A}^2A'$ PES. At E_{col} = 0.05 eV, for example, the RT σ_{A0}^H and σ_{A1}^H contribute by 13.2 and 15.8%, respectively, to the total RT depletion cross sections $\left(\sigma_{A j_0}^H + \sigma_{A j_0}^{H^+}\right)$ of $O + H_2^+$.

On the overall, at $E_{col} \geq 0.1$ eV both V^{RT} and C^{RT} increase a little the observable H/H^+ RT branching ratios $\sigma_{j_0}^H \Big/ \sigma_{j_0}^{H^+} = \left(\sigma_{X j_0}^H + \sigma_{A j_0}^H\right) \Big/ \left(\sigma_{X j_0}^{H^+} + \sigma_{A j_0}^{H^+}\right)$ with respect to the BO ones $\sigma_{X j_0}^H \Big/ \sigma_{A j_0}^{H^+}$. The largest variations occur at 0.1 eV, from the BO ratios of 2.38 and 2.28 at j_0 = 0 and 1, respectively, to the RT values equal to 2.71 at both j_0; that is a 13.9 or 18.9% of increasing at these rotational levels. This finding is essentially associated with $\sigma_{A j_0}^H$ that correspond to $\tilde{A}^2A' \rightarrow \tilde{X}^2A''$ nonadiabatic transitions. For the $\tilde{X}^2A''$ PES the main result arising from the RT effects is the lowering of the reactivity, as a consequence of the V^{RT} barrier, with a negligible production of the $OH + H^+$ nonadiabatic reaction channel. We close this discussion by plotting in Fig. 6 BO and RT averaged cross sections $\sigma_{j_0}^H = \left(\sigma_{X j_0}^H + \sigma_{A j_0}^H\right)/9$ and $\sigma_{j_0}^{H^+} = \left(\sigma_{X j_0}^{H^+} + \sigma_{A j_0}^{H^+}\right)/9$ with f_{el} = 1/9, at j_0 = 0 and 1. We clearly see the very small role of the H_2^+ rotational excitation and the H/H^+ product branching ratio in the E_{col} range investigated.

As stated in Section II, rate constants are obtained from RWP cross sections at $E_{col} \geq 0.05$ eV and from the extrapolated ones down to E_{col} = 0.005 eV *via* eqn (2.9). Table 3 and Fig. 7 are related to Table 2 and Fig. 6, respectively, and present the H and H^+ BO and RT rate constants $k_{e_0 j_0}$ and k_{j_0} from 200 to 900 K, with $k_{j_0}^H = k_{X j_0}^H + k_{A j_0}^H$ and $k_{j_0}^{H^+} = k_{X j_0}^{H^+} + k_{A j_0}^{H^+}$, with f_{el} = 1/9 and j_0 = 0 and 1. These data are consistent with the σ results for the H/H^+ branching ratio, for the reactivity of the initial electronic and rotational states, and for the BO or RT findings. All rate constants increase moderately with temperature. Regarding the BO results, k_{X0}^H is almost independent of T and $k_{A0}^{H^+}$ increases by 46% from 200 to 900 K. On the other hand, RT rate constants increase for both reaction channels by 38 and 91% for k_0^H and $k_0^{H^+}$, respectively. As expected, the V^{RT} and C^{RT} effects on the cross sections are confirmed for the rate constants: the former

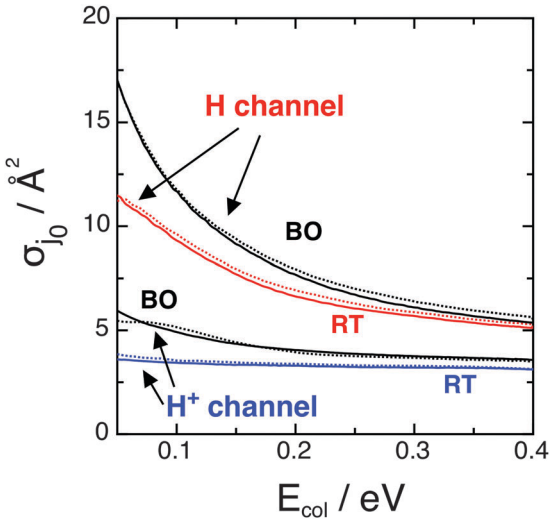

Fig. 6 BO (black) and RT (red and blue) CC averaged cross sections, j_0 = 0 (full) and 1 (dots), $E_{col} \geq 0.05$ eV, f_{el} = 1/9.

Table 3 H and H^+ BO and RT j_0 = 0 rate constants/10^{-10} cm^3 s^{-1} with f_{el} = 1/9

	H channel			H^+ channel		
	k_{X0}^H	k_{X0}^H	k_0^H	$k_{A0}^{H^+}$	$k_{A0}^{H^+}$	$k_0^{H^+}$
T/K	BO	RT	RT	BO	RT	RT
200	3.50	1.89	2.00	1.05	0.52	0.56
300	3.67	2.14	2.26	1.19	0.64	0.68
500	3.75	2.43	2.55	1.36	0.82	0.86
700	3.74	2.58	2.69	1.46	0.95	0.98
900	3.67	2.64	2.76	1.53	1.04	1.07

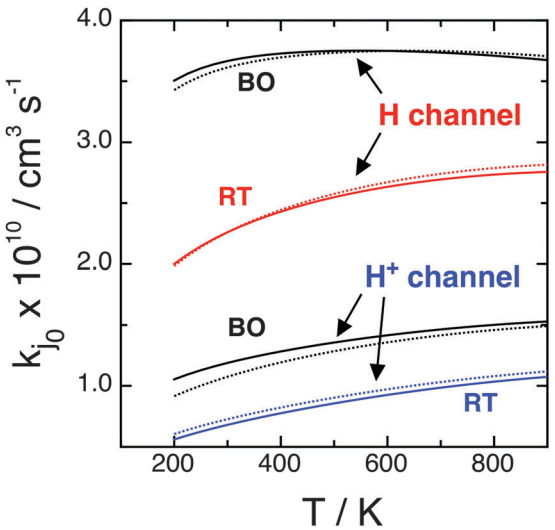

Fig. 7 BO (black) and RT (red and blue) CC rate constants, j_0 = 0 (full) and 1 (dots), f_{el} = 1/9.

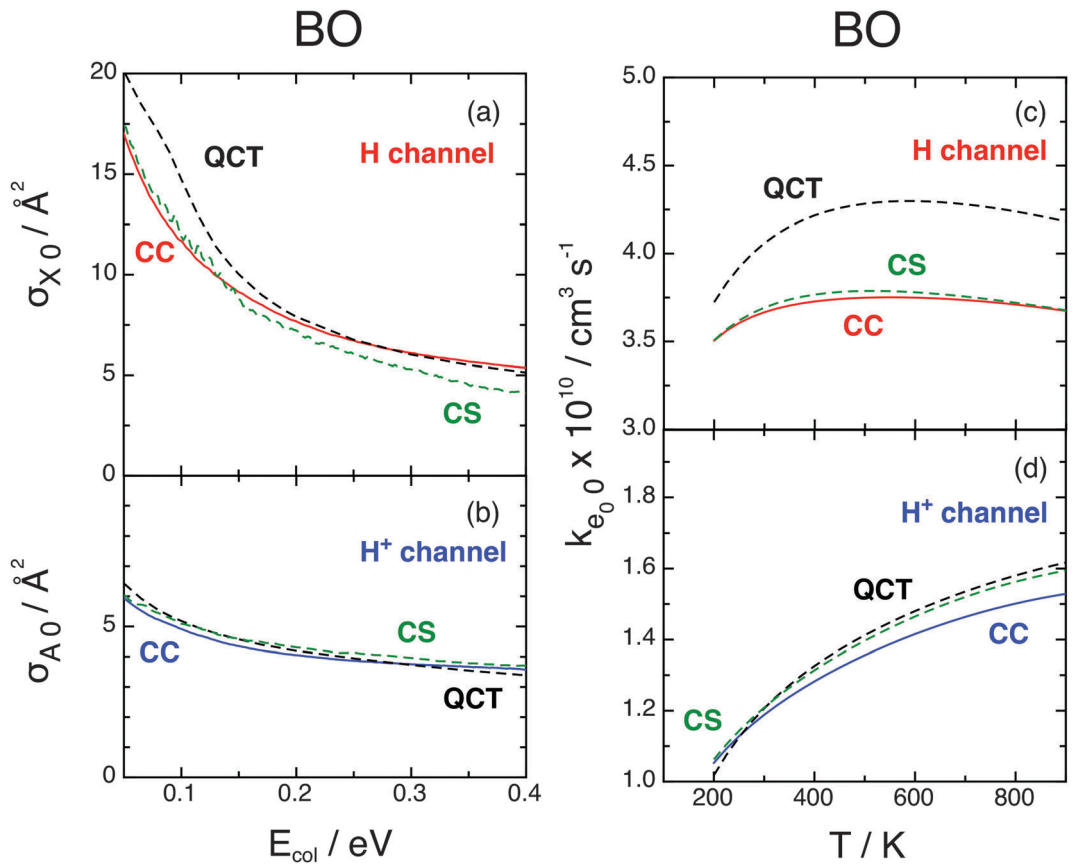

Fig. 8 BO cross sections (left, $E_{col} \geq 0.05$ eV) and rate constants (right), $e_0 = \tilde{X}^2A''$ (above) and $\tilde{A}^2A'$ (below), $j_0 = 0$, $f_{el} = 1/9$. CC (red and blue), CS (green), QCT (black). CS and QCT data from ref. 9.

nearly halves the reactivity at room T and the latter is rather small. Table 3 also shows that the RT $j_0 = 0$ branching ratio $k_0^H / k_0^{H^+}$ at 300 K is equal to 3.32 and a value of 3.10 is obtained for $j_0 = 1$. The differences between these values and the BO ones are of only ~8%, *i.e.*, less than one half of the cross-section values owing to the integration on E_{col}. Note that the large k^H values for the H channel imply that $O(^3P) + H_2^+(^2\Sigma_g^+) \rightarrow OH^+(X^3\Sigma^-) + H(^2S)$ is a highly reactive atom + diatom collision. In fact, at room temperature and at the RT level we have $k_0^H(300\ K) = k_1^H(300\ K) = 2.26 \times 10^{-10}$ cm^3 s^{-1} and this value is larger than that of similar RT reactive systems, namely 1.39×10^{-10} cm^3 s^{-1} for $C(^1D) + H_2(^1\Sigma_g^+)$[18] and 2.20×10^{-12} cm^3 s^{-1} for $N(^2D) + H_2(^1\Sigma_g^+)$.[19] The present H channel reaction (1.1) is so reactive owing to barrierless and strongly attractive character of the ground PES and to the larger exothermicity.

In Fig. 8 we compare the present BO CC cross sections and rate constants for $j_0 = 0$ with previous CS and QCT results,[9] with $f_{el} = 1/9$ everywhere. CC and CS data of both channels compare very well, as we have found for probabilities, whereas H-channel QCT results are slightly higher, implying that quantum effects are little important in the investigated reactions.[9]

Finally, we analyze the influence of the different choices (1), (2), and (3) of the $O(^3P)$ partition function presented at the end of Section II, plotting in Fig. 9 the associated RT rate constants $k_0 = k_{X0} + k_{A0}$ at $j_0 = 0$. We remember that (1) does not consider the $O(^3P)$ fine structure, which is taken into account by (2) and (3) with energy zero at the $O(^3P_2)$ state or at the $O(^3P)$ term, respectively. At not too large T values we have $f_{el}^{(2)} > f_{el}^{(1)} > f_{el}^{(3)}$ and, therefore, choices (2) and (3) present opposite effects: the former enhances whereas the latter inhibits k with respect to $f_{el}^{(1)}$. Moreover, $f_{el}^{(2)}$ decreases whereas $f_{el}^{(3)}$ increases with T. This behavior is confirmed in Fig. 9, where all rate constants increase with T, especially those of the H^+ channel, choices (1) and (3) give similar results, and k due to choice (2) is significantly larger. At 300 K k_0^H varies within (2.07–3.02) $\times 10^{-10}$ cm^3 s^{-1} and $k_0^{H^+}$ within (0.55–0.87) $\times 10^{-10}$ cm^3 s^{-1} according to the three choices of f_{el}, and these intervals increase at smaller T. These effects could be validated by further studies that consider the $O(^3P_M)$ fine structure at low temperatures.

V. Summary and conclusions

We have investigated the reactive collisions $O(^3P) + H_2^+(X^2\Sigma_g^+) \rightarrow OH^+(X^3\Sigma^-) + H(^2S)$, the H channel, and the $\rightarrow OH(X^2\Pi) + H^+$, H^+ channel, on the OH_2^+ $\tilde{X}^2A''$ and $\tilde{A}^2A'$ BO uncoupled or RT coupled PESs. Highly accurate MRCI PESs and $\hat{L}$ matrix elements, a CC quantum theory of RT atom + diatom collisions up to $J = 75$, and the time-dependent RWP and flux methods

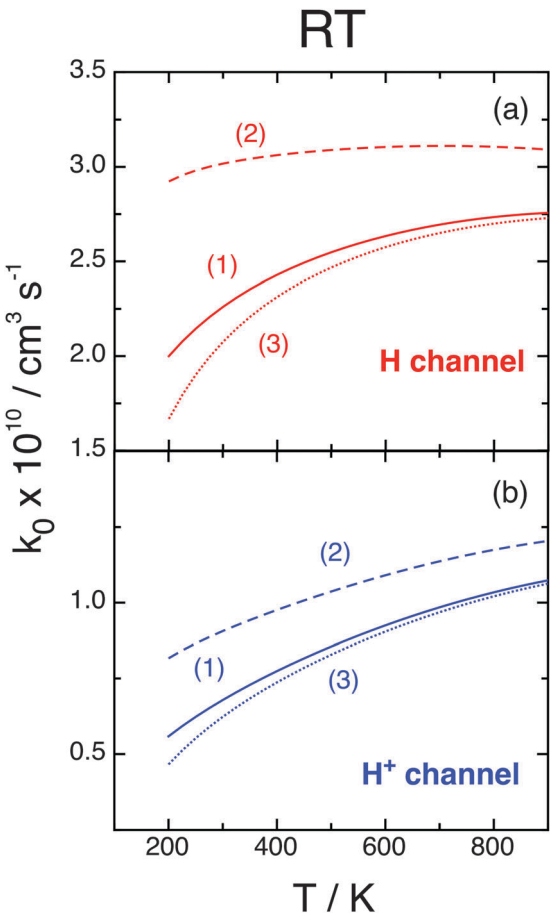

Fig. 9 RT rate constants, $j_0 = 0$, f_{el} from eqn (2.8) with $q_{el,O(^3P)}$ from choices (1), (2), and (3).

were employed. The electronic states are the degenerate components of a linear $^2\Pi$ species and are, therefore, strongly perturbed by RT effects due to $\hat{L}$, which modify the BO PESs and couple the electronic states *via* RT potentials V^{RT} (2.1) and couplings C^{RT} (2.2), respectively. The forms and roles of these RT terms are thoroughly discussed, pointing out that they describe the couplings among total rotation, electronic rotation, and angular motion. In particular, V^{RT} represents a dynamical and linear barrier added to the usual BO PES whereas C^{RT} couples the electronic states when $K > 0$.

The present RT CC work extends BO QCT and RWP CS studies on the uncoupled PESs reported recently by some of us,[8,9] showing that all the theoretical results agree rather well and give a common picture of the reaction dynamics. Thus, reaction probabilities are large and without threshold energy, the cross sections σ decrease with E_{col} from large threshold values, and the rate constants k show a small dependence with T, because the PESs are barrierless. The $\tilde{X}^2A''$ ground electronic state is more reactive up to a factor of $\sim$3, owing to its larger attractive character and exothermicity, the H product channel is thus favored, and the H_2^+ rotational excitation does not practically affect the σ and k values.

Owing to the repulsive collinear potentials V^{RT} (2.1), the RT energy thresholds are larger and the reaction probabilities are smaller than the BO ones. This finding is more evident for the $\tilde{A}^2A'$ excited state, owing to its $^2\Pi_u$ equilibrium geometry where the rotational constant B is large. The RT couplings C^{RT} (2.2) mix the electronic states up to $\sim$20% and are more important when the WP starts on the excited PES at low J values and $K_0 = 0$. These couplings, however, decrease quickly at high J values and, on the overall, the reactivity is inhibited when K_0 and/or $K = 0$. These results are explained by considering the expressions of the diagonal and off-diagonal RT terms, the linear values of the initial Legendre functions, and the good agreement between BO CC and CS probabilities at $K_0 = 0$, which implies that the collision dynamics does not appreciably modify the initial K_0 value. RT effects smooth the $\sigma(E_{col})$ curves with respect to the BO ones and the RT diagonal barriers V^{RT} nearly halve the σ and k values at low energy and room temperature. The RT nonadiabatic couplings C^{RT} modify these observables and the H/H^+ product branching ratios up to $\sim$19% with respect to the BO ones. The collision $O(^3P) + H_2^+(X^2\Sigma_g^+) \rightarrow OH^+(X^3\Sigma^-) + H(^2S)$ is highly reactive, as it comes out from $k_{j_0}(300) = 2.26 \times 10^{-10}$ cm^3 s^{-1}.

In summary, we note that other nonadiabatic interactions could be important for the collisional dynamics in OH_2^+ and deuterated variants at low energies. Looking at the correlation diagrams of Fig. 1 and to those more detailed in ref. 8 and 11, we see for example:

(1) A RT-induced charge-transfer quenching (q), $OH(X^2\Pi) + D^+ \rightarrow OH^+(X^3\Sigma^-) + D$, and an exchange-quenching (eq), $OH(X^2\Pi) + D^+ \rightarrow OD^+(X^3\Sigma^-) + H$, which are in competition with the exchange process (e), $OH(X^2\Pi) + D^+ \rightarrow OD(X^2\Pi) + H^+$, but not with the formation of $O(^3P) + HD^+$ that is closed below $E_{col} = 1.62$ eV. Preliminary results suggest a branching ratio [(q) + (eq)]/(e) greater than one, that is significant RT effects larger than those in $O(^3P) + H_2^+$.

(2) A $\tilde{B}^2B_2 - \tilde{A}^2A_1$ conical intersection (CI) in the $O(^3P) + H_2^+(X^2\Sigma_g^+)$ arrangement, which might decrease the efficiency of the present reactions, mainly for the H^+ channel, opening a third product channel, $OH^+(a^1\Delta) + H(^2S)$. We plan to investigate this point in a nonadiabatic future work considering $\tilde{X} - \tilde{A} - \tilde{B}$ three-state CI and RT effects.

On the other hand, intersystem-crossing effects among the $\tilde{a}^4A''$ quartet, shown in Fig. 1 of ref. 8 and 11, and the $\tilde{X}^2A''$ and $\tilde{A}^2A'$ doublets are not expected to be important, taking into account the $O(^3P,^1D) + H_2(X^1\Sigma_g^+)$[35] and $O^+(^4S) + H_2(X^1\Sigma_g^+)$[36] dynamical studies.

Acknowledgements

This work was supported by the Spanish Ministry of Science and Innovation (MICINN projects CTQ2011-27857-C02-01 and CONSOLIDER INGENIO 2010 under grant no. CSD2009-00038 entitled ''Molecular Astrophysics: the Herschel and Alma era''). Thanks are also given to the ''Generalitat de Catalunya'' (Autonomous Government of Catalonia; refs. 2014SGR 25, 2014SGR 1582 and XRQTC) for some help. We gratefully acknowledge H. Guo and D. Xie for the matrix elements of the electronic angular momenta.

References

1 P. A. Wehinger, S. Wickoff, G. Herzberg and H. Lew, *Astrophys. J.*, 1974, **190**, L43.
2 W. T. Huntress Jr., *Astrophys. J., Suppl. Ser.*, 1977, **33**, 495.
3 G. Herzberg, *Ann. Geophys.*, 1980, **36**, 605.
4 E. F. Van Dishoeck, E. Herbst and D. A. Neufeld, *Chem. Rev.*, 2013, **113**, 9043.
5 P. Gamallo, F. Huarte-Larrañaga and M. González, *J. Phys. Chem. A*, 2013, **117**, 5393.
6 R. Martínez, J. D. Sierra, S. K. Gray and M. González, *J. Chem. Phys.*, 2006, **125**, 164305.
7 D. J. McClure, C. H. Douglas and W. R. Gentry, *J. Chem. Phys.*, 1977, **67**, 2362.
8 M. Paniagua, R. Martínez, P. Gamallo and M. González, *Phys. Chem. Chem. Phys.*, 2014, **16**, 23594.
9 R. Martínez, M. Paniagua, J. Mayneris-Perxachs, P. Gamallo and M. González, *Phys. Chem. Chem. Phys.*, under revision.
10 M. A. Gannouni, N. E. Jaidane, P. Halvick, T. Stoecklin and M. Hochlaf, *J. Chem. Phys.*, 2014, **140**, 184306.
11 K. T. Gillen, B. H. Mahan and J. S. Winn, *J. Chem. Phys.*, 1973, **58**, 5373.
12 M. Brommer, B. Weis, B. Follmeg, P. Rosmus, S. Carter, N. C. Handy, H.-J. Werner and P. J. Knowles, *J. Chem. Phys.*, 1993, **98**, 5222.
13 J. Suárez, L. Méndez and I. Rabadán, *J. Phys. Chem. Lett.*, 2015, **6**, 72.
14 S. Zhou, Z. Li, D. Xie, S. Y. Lin and H. Guo, *J. Chem. Phys.*, 2009, **130**, 184307.
15 S. H. Lin, H. Guo, B. Jiang, S. Zhou and D. Xie, *J. Phys. Chem. A*, 2010, **114**, 9655.
16 C. Petrongolo, *J. Chem. Phys.*, 1988, **89**, 1297.
17 P. Defazio and C. Petrongolo, *J. Chem. Phys.*, 2006, **125**, 064308.
18 P. Defazio, B. Bussery-Honvault, P. Honvault and C. Petrongolo, *J. Chem. Phys.*, 2011, **135**, 114308.
19 P. Gamallo, P. Defazio, M. González and C. Petrongolo, *J. Chem. Phys.*, 2008, **129**, 244307.
20 P. Gamallo, S. Akpinar, P. Defazio and C. Petrongolo, *J. Chem. Phys.*, 2013, **139**, 094303.
21 S. K. Gray and G. G. Balint-Kurti, *J. Chem. Phys.*, 1998, **108**, 950.
22 A. J. H. M. Meijer, E. M. Goldfield, S. K. Gray and G. G. Balint-Kurti, *Chem. Phys. Lett.*, 1998, **293**, 270.
23 R. Chen and H. Guo, *J. Chem. Phys.*, 1996, **105**, 3569.
24 G.-J. Kroes and D. Neuhauser, *J. Chem. Phys.*, 1996, **105**, 8690.
25 S. Y. Lin and H. Guo, *Phys. Rev. A: At., Mol., Opt. Phys.*, 2006, **74**, 022703.
26 NIST *Atomic Spectra Database Levels*, http://physics.nist.gov/PhysRef Data/ASD/levels_form.html.
27 F. Matzkies and U. Manthe, *J. Chem. Phys.*, 1998, **108**, 4828.
28 U. Manthe, G. Capecchi and H.-J. Werner, *Phys. Chem. Chem. Phys.*, 2004, **6**, 5026.
29 P. Gamallo, R. Francia, R. Martínez, R. Sayós and M. González, *J. Phys. Chem. A*, 2012, **116**, 11783.
30 P. Gamallo, S. Akpinar, P. Defazio and C. Petrongolo, *J. Phys. Chem. A*, 2014, **118**, 6451.
31 D. De Fazio, *Phys. Chem. Chem. Phys.*, 2014, **16**, 11662.
32 D. Skouteris, J. F. Castillo and D. E. Manolopoulos, *Comput. Phys. Commun.*, 2000, **133**, 128.
33 P. Gamallo, F. Huarte-Larrañaga and M. González, *J. Phys. Chem. A*, 2013, **117**, 5393.
34 R. D. Levine and R. B. Bernstein, *Molecular Reaction Dynamics and Chemical Reactivity*, Oxford University Press, Oxford, 1987, p. 58.
35 T.-H. Chu, X. Zhang and K.-L. Han, *J. Chem. Phys.*, 2005, **122**, 214301and references therein.
36 R. Martínez, J. D. Sierra, S. K. Gray and M. González, *J. Chem. Phys.*, 2006, **125**, 164305, and references therein.